The Effect of Strong Heat Addition on the Convergence of Implicit Schemes

Charles L. Merkle,* Anil Gulati,† and Yun-Ho Choi†
The Pennsylvania State University, University Park, Pennsylvania

The effect of substantial amounts of heat addition on the convergence characteristics of implicit algorithms for flow in a converging-diverging nozzle is investigated. Heat addition has an adverse effect on convergence because it decreases the Mach number at the inlet, introduces a strong energy source term, and produces steep temperature gradients. The nozzle convergence rate has analogous detrimental effects and is also studied. Comparisons of both variations show that when equivalent procedures are used, Beam and Warming's algorithm converges for somewhat wider ranges of parameters than does MacCormack's. The combination of local time steps which provide uniform values of CFL throughout the grid, boundary conditions based on the method of characteristics, and Euler implicit differencing in time provides convergence that is nearly independent of heat addition and is in close agreement with the predictions of stability theory. The incorporation of real gas effects was tested and shown to have a minor effect.

Introduction

MOST current computational efforts are directed toward problems in which there is no significant heat transfer. There are, however, a large number of problems in which heat addition (or removal) is a dominant feature. Some examples include diffusion flames, droplet burning, and flow through a turbine with heat transfer to the blades. The present study is stimulated by yet another problem in which the governing feature of the flow is the heat added through absorption of laser energy. This problem arises from a potential new concept for spacecraft propulsion for which accurate numerical simulations of the flowfield are urgently needed to guide ongoing experiments.[1] Although the amount of heat added per unit volume of gas in the laser propulsion application is considerably higher than in the other applications noted above, it is anticipated that the findings of the present study will be useful for these other areas as well.

A laser-powered thruster is completely analogous to a conventional chemical propulsion engine, except an "absorber" is used to convert the radiant energy in the beam to internal kinetic energy of the gas. The hot gas is then expanded through a conventional convergent-divergent nozzle to produce thrust. Thus far, most of the analytical and computational efforts concerning this problem have been directed toward obtaining solutions of an approximate steady-state equation in which the mass flow rate emerges as an eigenvalue.[2-4] However, these simplifications omit some of the significant physics of the problem. A time-marching numerical solution of the full Navier-Stokes equations for this problem appears to be the most promising approach for obtaining accurate steady-state predictions which include the dominant physics. Such a simulation involves considerable difficulties due to the large amount of heat absorbed by the gas and the strong interaction between the flowfied and the incoming laser beam.[5] Thus, for the purposes of the present study, this nonlinear coupling has been replaced by a specified heat addition. This allows emphasis to be placed on the effect of large heating rates on the convergence of the numerical scheme. For similar reasons, the present effort is directed toward the quasi-one-dimensional problem even though the physical problem is highly two-dimensional.

In studying this problem, a number of different algorithms have been considered, but prime attention has been centered on an Euler implicit scheme such as that of Beam and Warming[6] and on the bidiagonal implicit scheme of MacCormack.[7] The general observation is that all methods work adequately at low heating rates, but become less reliable at higher heating rates. Extreme care must be used to get any of the methods in the literature to converge successfully at the maximum heating rates of interest for the laser propulsion problem. Similar trends are also observed for nozzles without heat addition, but with large convergence ratios. This sensitivity can be attributed to the large source terms which appear in the problem and the accompanying complications they cause including low inlet Mach numbers, steep temperature profiles, and strongly varying Jacobians throughout the flowfield.

Although the gases are no longer calorically perfect at the temperature of interest, for simplicity and clarity, the calculations presented are for a constant property gas. However, the equations are developed for a variable property gas.

Governing Equations

The Navier-Stokes equations for quasi-one-dimensional flow are given in weak conservation form as

$$\frac{\partial U}{\partial t}+\frac{\partial F'}{\partial x}(U)=H \tag{1}$$

where the vectors U and H are defined as

$$U=A_F\begin{bmatrix}\rho\\ \rho u\\ e\end{bmatrix} \text{ and } H=\begin{bmatrix}0\\ p\mathrm{d}A_F/\mathrm{d}x\\ QA_F\end{bmatrix} \tag{2}$$

The vector F' is defined as

$$F'=A_F\begin{bmatrix}\rho u\\ \rho u^2+\sigma\\ (e+\sigma)u-kT_x\end{bmatrix} \tag{3}$$

Presented as Paper 83-1914 at the AIAA Computational Fluid Dynamics Conference, Danvers, Mass., July 13-15, 1983; received Aug. 26, 1983; revision received June 14, 1984.

*Professor, Mechanical Engineering. Member AIAA.
†Graduate Assistant, Mechanical Engineering.

where $\sigma = p - (\lambda + 2\mu)du/dx$. For convenience, F' can be split into inviscid and viscous parts, F and V, as

$$F' = F + V \tag{4}$$

In the above equations, A_F represents the nozzle flow area and Q the heat addition per unit volume, while the remaining variables are defined by standard notation, including: density ρ, velocity u, total energy per unit volume e, temperature T, pressure p, viscosity coefficients μ and λ, and thermal conductivity k.

The specific internal energy ϵ, which can be expressed as a function of the temperature and pressure, $\epsilon = \epsilon(T,p)$, is related to the total energy by

$$\epsilon = e/\rho - u^2/2 \tag{5}$$

For an equilibrium gas, the equation of state is,

$$p = \rho RT/M \tag{6}$$

where the molecular weight M also depends on temperature and pressure, $M = M(T,p)$.

The functional relations for the internal energy and molecular weight must be obtained from thermodynamic data for the gas chosen. For the laser thruster problem, hydrogen is frequently the preferred working fluid. Consequently, the calculations in the present paper are based upon the properties of hydrogen.

As indicated in Eqs. (1) and (2), both the momentum and energy equations have nonzero source terms. The source in the momentum equation is dictated by the nozzle area change, while the energy source is taken as a specified function of the independent variable, $Q = Q(x)$ [whereas in the laser problem, it depends upon the dependent variable, $Q = Q(u)$].

For the real gas case, the Jacobian of the inviscid flux vector, F, is defined as $A = \partial F/\partial U$, and is given by

$$A = \begin{bmatrix} 0 & 1 & 0 \\ \alpha\dfrac{RT}{M} + \beta\left(u^2 - \dfrac{e}{\rho}\right)\alpha - u^2 & u(2-\beta\alpha) & \beta\alpha \\ \alpha u\left[\dfrac{RT}{M} + \beta\left(u^2 - \dfrac{e}{\rho}\right)\right] & \dfrac{e+p}{\rho} - \beta\alpha u^2 & u(1+\beta\alpha) \\ -u(e+p)/\rho & & \end{bmatrix} \tag{7}$$

where R is the universal gas constant and α and β parameters which are defined as

$$\alpha = \left[1 + \rho\beta\left(\frac{\partial \epsilon}{\partial p}\right)_T + \frac{P}{M}\left(\frac{\partial M}{\partial p}\right)_T\right]^{-1} \tag{8}$$

and

$$\beta = \frac{R}{Mc_v}\left[1 - \frac{T}{M}\left(\frac{\partial M}{\partial T}\right)_p\right] \tag{9}$$

For the ideal gas case, α reduces to unity, while β reduces to $\gamma - 1$.

Equation (1) can be transformed to characteristic form by premultiplying by a specific matrix S^{-1} to give

$$\frac{\partial \hat{U}}{\partial t} + \Lambda\frac{\partial \hat{U}}{\partial x} = S^{-1}H \tag{10}$$

where Λ is the diagonal matrix

$$\Lambda = \text{diag}(u, u+c, u-c) \tag{11}$$

which is obtained from the similarity transformation

$$\Lambda = S^{-1}AS \tag{12}$$

Here, c is the speed of sound defined as $c^2 = p(1+\beta)\alpha/\rho$. The characteristic variables in Eq. (10) are defined as

$$d\hat{U} = S^{-1}dU \tag{13}$$

This form of the equation is used in applying boundary conditions.

The matrix S^{-1} is defined as $S^{-1} = T^{-1}M^{-1}$. The matrix M^{-1} transforms the conservative form of the equations to the quasilinear form, while T^{-1} transforms the quasilinear equations to characteristic form:

$$M^{-1} = \begin{bmatrix} 1 & 0 & 0 \\ -u/\rho & 1/\rho & 0 \\ \alpha(P/\rho) - \alpha\beta(\epsilon - u^2/2) & -\alpha\beta u & \alpha\beta \end{bmatrix} \tag{14}$$

and

$$T^{-1} = \begin{bmatrix} 1 & 0 & -1/c^2 \\ 0 & \rho c & 1 \\ 0 & -\rho c & 1 \end{bmatrix} \tag{15}$$

To complete the analysis, the Jacobian for the source vector H is given by

$$D = \frac{\partial H}{\partial U} = \frac{1}{A_F}\begin{bmatrix} 0 & 0 & 0 \\ \dfrac{dA_F}{dx}\left(\dfrac{RT}{M}\right) + \beta\left(u^2 - \dfrac{e}{\rho}\right) & -u\beta\dfrac{dA_F}{dx} & \beta\dfrac{dA_F}{dx} \\ 0 & 0 & 0 \end{bmatrix} \tag{16}$$

Similarly, the Jacobians for the viscous flux vector can be found. All of these Jacobians, matrices and equations reduce to their familiar perfect gas forms by replacing β with $\gamma - 1$ and α by unity.

Method of Solution

A number of implicit schemes are available for the Navier-Stokes equations.[8] The present calculations are based primarily upon the methods of Beam and Warming[6] and MacCormack,[7] although the methods of Steger and Warming[9] and Briley and McDonald[10] have also been tested. Accordingly, the former two methods are outlined here with emphasis on their similarities and differences.

Beam and Warming's Implicit Scheme

The Beam and Warming scheme discussed in detail in Refs. 6 and 11 has been widely used.[6,12] Applying Beam and Warming's method to Eq. (1) and expressing in delta form gives

$$\left\{I + \frac{\theta\Delta t}{1+\xi}\left[\frac{\partial}{\partial x}(A - P + R_x)^n - \frac{\partial^2}{\partial x^2}R^n - D^n\right]\right\}\Delta U^n = \frac{\Delta t}{1+\xi}\left[\frac{\partial}{\partial x}(-F^n + V^n) + H^n\right] + \frac{\xi}{1+\xi}\Delta U^{n-1} \tag{17}$$

where the Jacobians, A, P, R, and D are as defined earlier. In this form, Eq. (17) represents an entire class of differencing schemes, depending on the values chosen for θ and ξ.[6] In the present analysis, θ was taken as 1 and ξ was taken as 0, leading to the two-point Euler implicit backward difference.

In evaluating Eq. (17), the spatial derivatives are central differenced resulting in a block tridiagonal system. This scheme, like MacCormack's, is second-order accurate in space. In contrast to MacCormack's scheme, where the viscous terms are treated by Saul'ev's method,[13] the viscous terms in Beam and Warming's algorithm can be included by standard differencing techniques without altering the matrix structure (which is already block tridiagonal). The source terms are also treated fully implicitly as indicated in Eq. (17).

MacCormack's Implicit Scheme

MacCormack's implicit algorithm is based upon adding an implicit correction to his well-known explicit scheme.[14] This correction makes direct use of a modified set of eigenvalues of the Jacobian of the flux vectors. The implicit system retains the alternate type differencing distinctive of the original explicit scheme and leads to a block bidiagonal system. When MacCormack's scheme is applied, Eq. (1) takes the following implicit predictor-corrector form:

Predictor form:

$$\Delta U_i^n = \frac{-\Delta t}{\Delta x}\Delta_+ F_i^n + \frac{\Delta t}{2}(H_i^n + H_{i+1}^n) \tag{18a}$$

$$\left[I - \frac{\Delta t}{\Delta x}\Delta_+ A^*\right]\delta\overline{U_i^{n+1}} = \Delta U_i^n \tag{18b}$$

$$\overline{U_i^{n+1}} = U_i^n + \delta\overline{U_i^{n+1}} \tag{18c}$$

Corrector form:

$$\Delta\overline{U_i^{n+1}} = -\frac{\Delta t}{\Delta x}\Delta_- \overline{F_i^{n+1}} + \frac{\Delta t}{2}(\overline{H_i^{n+1}} + \overline{H_{i-1}^{n+1}}) \tag{19a}$$

$$\left[I + \frac{\Delta t}{\Delta x}\Delta_- A^*\right]\delta U_i^{n+1} = \Delta\overline{U_i^{n+1}} \tag{19b}$$

$$U_i^{n+1} = \tfrac{1}{2}(U_i^n + \overline{U_i^{n+1}} + \delta U_i^{n+1}) \tag{19c}$$

where Δ_+ and Δ_- represent forward and backward differences, respectively, and A^* is the Jacobian with modified eigenvalues defined below.

The modified Jacobian A^* is related to the original matrix A by a similarity transformation of a modified set of eigenvalues. Thus, in creating the modified matrix A^*, the diagonal matrix Λ is altered from the viscous counterpart of Eq. (10) to a new matrix Λ^* given by

$$\Lambda^* = \text{diag}(\lambda_1^*, \lambda_2^*, \lambda_3^*) \tag{20}$$

where

$$\lambda_1^* = \max\left(|u| + \frac{2\mu}{\rho\Delta x} - \frac{1}{2}\frac{\Delta x}{\Delta t},\ 0\right)$$

$$\lambda_2^* = \max\left(|u+c| + \frac{2\mu}{\rho\Delta x} - \frac{1}{2}\frac{\Delta x}{\Delta t},\ 0\right)$$

$$\lambda_3^* = \max\left(|u-c| + \frac{2\mu}{\rho\Delta x} - \frac{1}{2}\frac{\Delta x}{\Delta t},\ 0\right) \tag{21}$$

The matrix A^* is then

$$A^* = S\Lambda^* S^{-1} \tag{22}$$

where S is as given earlier.

The treatment of the source terms also requires comment. The source term in the energy equation is independent of the solution vector U [see Eq. (16)]. Thus, its treatment can neither be described as being implicit nor explicit. The source term in the momentum equation, however, does contribute to the Jacobian D and requires a choice of either implicit or explicit differencing. Since the similarity transform which diagonalizes D is different from the one that diagonalizes A, it is not possible to treat this source term implicitly without destroying the block bidiagonal structure of the method.[15] Stability results shown later suggest that explicit treatment of the source term has little effect.

Viscous Dissipation and Stability Considerations

Experience with these two methods shows MacCormack's scheme is sufficiently dissipative to obviate the need for additional damping. Such is not the case with Beam and Warming's algorithm which requires the addition of artificial viscosity to maintain stability. The difference between the two algorithms arises because of their differing treatment of the advection terms. To remove the stability limitations in Beam and Warming's algorithm, two types of artificial viscosity were incorporated as recommended by Steger and Bailey.[12] These include a second-order viscosity that is differenced implicitly, and a fourth-order term that is differenced explicitly. To understand the impact of these added terms, and to anticipate the convergence characteristics, a brief stability analysis of both methods is included. For simplicity in these analyses, the inviscid equations with constant property are used and the Jacobians of the flux vectors are taken to be locally constant.

Stability of Beam and Warming's Algorithm

The analysis of Beam and Warming's Euler implicit method begins by adding artificial viscosity terms in differential form. Thus, the numerical solution of the modified equations is considered as

$$\frac{\partial U}{\partial t} + \frac{\partial F}{\partial x} - \frac{\epsilon_i}{4}\Delta x^2 \frac{\partial^3 U}{\partial t \partial x^2} = H - \frac{\epsilon_e \Delta x^4}{8\Delta t}\frac{\partial^4 U}{\partial x^4} \tag{23}$$

Here, ϵ_i represents an implicit artificial viscosity, while ϵ_e represents an explicit viscosity.[12] Both of these quantities are

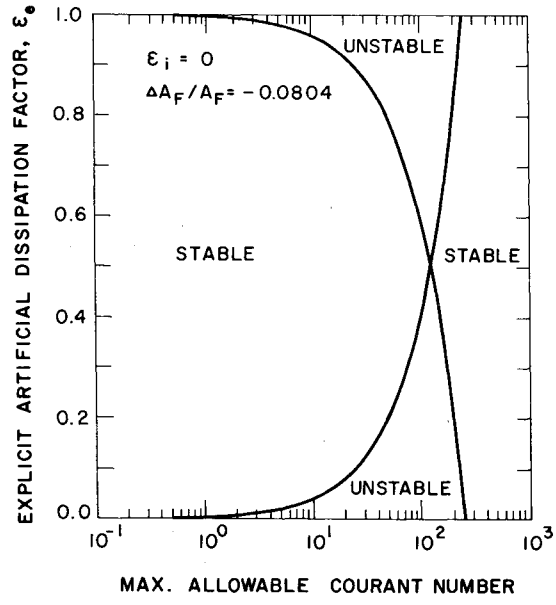

Fig. 1 Effect of explicit artificial dissipation on the maximum allowable Courant number for Beam and Warming's Euler implicit scheme.

pure numbers (no dimensions) that have been scaled to be of order 1. As can be seen, the effects of the implicit term vanish in the steady state, while those of the explicit term remain. The magnitude of the explicit viscosity is proportional to Δx^4, and is inversely proportional to the time step. Thus, the effect of the viscosity decreases rapidly with grid refinement, although the final solution is weakly dependent on the time step.

Applying Euler implicit differencing to all terms in Eq. (23), except the explicit viscosity term which is differenced at the old time level, we obtain:

$$\left[I+\Delta t\frac{\partial A}{\partial x}-\frac{\epsilon_i\Delta x^2}{4}\frac{\partial^2}{\partial x^2}-\Delta tD\right]U^{n+1}$$

$$=\left[I-\frac{\epsilon_i\Delta x^2}{4}\frac{\partial^2}{\partial x^2}-\frac{\epsilon_e\Delta x^4}{8}\frac{\partial^4}{\partial x^4}\right]U^n \tag{24}$$

which can be written in the symbolic form:

$$K_1U^{n+1}=K_2U^n \tag{25}$$

where K_1 and K_2 are the matrices obtained by central differencing all terms inside the brackets in Eq. (24).

The stability characteristics of the Euler implicit algorithm are determined by the eigenvalues of the matrix $K_1^{-1}K_2$. Solving for these eigenvalues in the high wave number limit shows that the amplification ratio is less than unity if the larger of the two following conditions is met:

$$\epsilon_e\geq 0 \text{ or } \epsilon_e\geq-\frac{\gamma-1}{2}\lambda_u\frac{\Delta A_F}{A_F} \tag{26a}$$

and if the smaller of

$$\epsilon_e\leq 1+\epsilon_i \text{ or } \epsilon_e\leq 1-\frac{\gamma-1}{2}\lambda_u\frac{\Delta A_F}{A_F}+\epsilon_i \tag{26b}$$

is met. In these expressions, $\lambda_u=u\Delta t/\Delta x$ is the CFL ratio based upon u, and ΔA_F the change of flow area between two grid points.

The stability criteria in these equations are interpreted graphically on Fig. 1 for one nozzle convergence rate, $\Delta A_F/A_F$, that is representative of conditions used in the present calculations. For clarity, only the results for zero implicit artificial viscosity ($\epsilon_i=0$) are shown. The addition of implicit viscosity simply shifts the top curve upward, as seen from Eq. (26b). For the particular area change ($\Delta A_F/A_F$) chosen, there is a range of CFL values for which the scheme is unstable. Below and above these values the scheme is again stable. The extent of this region depends upon the magnitude of ϵ_e. When $\epsilon_e=0.5$ (for $\epsilon_i=0$), this region shrinks to a point. Nevertheless, the large values of CFL to the right of the curves on Fig. 1 cannot be used for nozzle calculations. In a converging nozzle, $\Delta A_F/A_F$ takes on a sequence of values ranging from a maximum where the area is changing most rapidly to zero at the throat. The stability map for the nozzle is thus composed of a series of curves such as in Fig. 1, with the intersecting curves being pushed farther to the right as $\Delta A_F/A_F$ decreases. Thus, the region to the right of the curves in Fig. 1 will be unstable for smaller values of $\Delta A_F/A_F$ than the one shown. Only the region to the left of the intersecting curves can be used.

In this context, it is useful to note that an alternative viscosity coefficient could be defined that would minimize this dependence upon CFL, although it causes the viscosity to depend upon the solution as well as its derivative. The last term in Eq. (23) could be replaced by

$$-\frac{\epsilon'\Delta x^3 u}{8}\frac{\partial^4 U}{\partial x^4} \tag{27}$$

which removes the λ_u from the stability condition analogous to Eqs. (26) with ϵ' replacing ϵ. The resulting solution contains differing amounts of artificial viscosity at different regions in the flowfield.

Stability of MacCormack's Algorithm

MacCormack's differencing gives rise to a much more complicated stability relation. Using notation like that given above, we can collapse Eqs. (18) and (19) to give

$$(I-\lambda A^*\Delta_+)(\overline{U^{n+1}}-U^n)=-\lambda A\Delta_+U^n$$

$$+(\Delta t/2)D(U+U_{i+1})^n \tag{28a}$$

and

$$(I+\lambda A^*\Delta_-)(2U^{n+1}-\overline{U^{n+1}}-U^n)=-\lambda\Delta_-A\overline{U^{n+1}}$$

$$+(\Delta t/2)D(U+U_{i-1})^{\overline{n+1}} \tag{28b}$$

where λ is used here to denote $\Delta t/\Delta x$. As before, these can be placed in the simpler form,

$$K_1\overline{U^{n+1}}=K_2U^n \tag{29a}$$

$$K_3U^{n+1}=K_4U_n+K_5\overline{U^{n+1}} \tag{29b}$$

where the matrices are obtained from the indicated differencing in Eqs. (28), along with a Fourier decomposition. For this case, these matrices are:

$$K_1=I+\lambda(1-c-is)A^*$$

$$K_2=I+\lambda(1-c-is)(A^*+A)+(\Delta t/2)D(1+c+is)$$

$$K_3=I+\lambda(1-c+is)A^*$$

$$K_4=\tfrac{1}{2}[I+\lambda(1-c+is)A^*]$$

$$K_5=\tfrac{1}{2}[I+\lambda(1-c+is)(A^*-A)+(\Delta t/2)D(1+c-is)] \tag{30}$$

where the quantities c and s refer to the cosine and sine of the Fourier argument, respectively, and $i=\sqrt{-1}$. In the short wavelength limit where the Fourier argument approaches π (where $c=-1$ and $s=0$), it is readily seen that Eqs. (29) become independent of the Jacobian of the source term, D. Hence, the area change does not affect the stability of MacCormack's scheme at short wavelengths. Numerical calculations of the eigenvalues of Eqs. (29) likewise show the scheme is stable at other wavelengths as well for the area changes of interest.

Boundary Conditions

One-dimensional flow through a nozzle requires the specification of boundary conditions at the upstream and downstream ends. In the present problem, the flow is choked with supersonic flow downstream of the throat. The hyperbolic character of the flow at the exit simplifies the downstream boundary condition. A first-order implicit extrapolation in conserved variables,

$$U_{IL}^{n+1}=U_{IL-1}^{n+1} \tag{31}$$

(where $n+1$ is the new time level and IL the last grid point) proved to be adequate for all schemes tested. These boundary conditions reflect the physical (and mathematical) observation that all information at the downstream boundary should come from inside the domain.

Since the flow at the inlet is subsonic, the upstream boundary conditions exert a large influence on the solutions and its convergence. Subsonic inflow requires that two variables be specified to replace the two characteristics com-

ing from outside the domain. For both computational methods the stagnation pressure p^0 and stagnation enthalpy h^0 were chosen to provide this external information. However, the information from inside the domain was obtained from different procedures. For Beam and Warming's algorithm, the method of characteristics procedure outlined in Refs. 16 and 17 was used. The equations were written in the form given in Eq. (10), and the information from the first two equations was replaced by the conditions that p^0 and h^0 were constant. This procedure can be expressed formally by differentiating the (constant) boundary condition vector, $\Omega=\Omega(p^0, T^0, 0)^T$, to obtain two conditions for the change in the solution ΔU at the upstream end

$$\frac{\partial\Omega}{\partial U}\Delta U=0 \tag{32}$$

The third condition is obtained by multiplying Eq. (10) by the selection matrix, $L^-=\text{diag}(0,0,1)$. The three equations at the upstream boundary are then obtained by adding these two relations to give

$$\left\{L^-S^{-1}\left[I+\Delta t\left(\frac{\partial}{\partial x}A-D\right)\right]+\frac{\partial\Omega}{\partial Q}\right\}\Delta Q$$

$$=-L^-S^{-1}\Delta t\left\{\frac{\partial F}{\partial x}-H\right\} \tag{33}$$

This approach could not used with MacCormack's scheme because of its bidiagonal nature. Consequently, for MacCormack's scheme, the stagnation pressure and enthalpy, p^0 and h^0, were again specified from outside the domain, but the third condition was obtained by a second-order accurate implicit extrapolation of the velocity u

$$u_1^{n+1}=2u_2^{n+1}-u_3^{n+1} \tag{34}$$

from inside the domain. The extrapolation of velocity lacks rigorous physical basis, but proved to be acceptable. Other boundary conditions were not tried, but an implicit extrapolation of this type was tested in Beam and Warming's scheme and was shown to have only minor effects on convergence.

Numerical Results

As indicated previously, the computational results presented herein are for hydrogen gas flowing through a choked convergent-divergent nozzle. The main thrust of the calculations is to identify a method that will work successfully at heating rates corresponding to laser propulsion. Consequently, more emphasis has been placed on how reliably specific algorithms converge to a steady solution than on comparing the efficiency of computation of the various schemes. Because of the similarity in the flowfields,

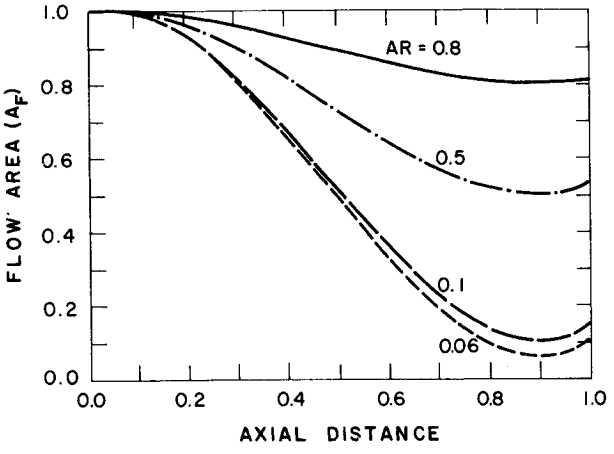

Fig. 2 Nozzle profile for various area ratios.

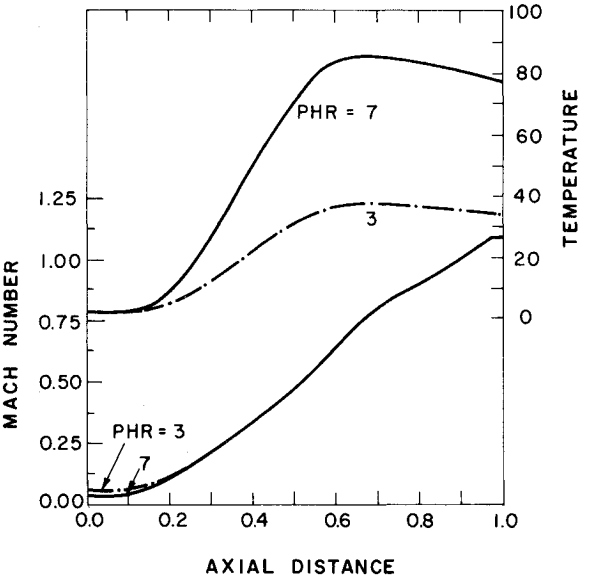

Fig. 4 Temperature profiles and Mach number profiles for peak heating rates of 3 and 7 for Beam and Warming's Euler implicit scheme, $\mathcal{R}=0.8$.

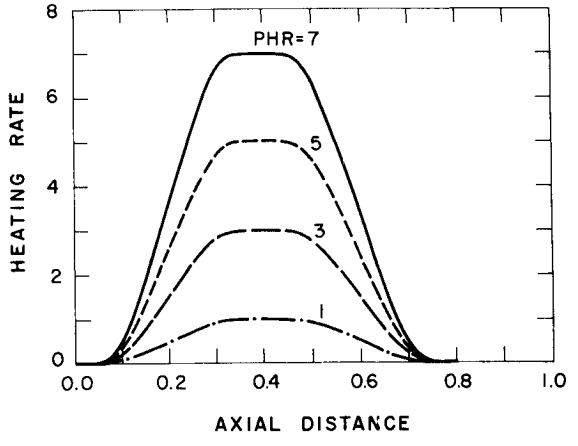

Fig. 3 Heating rate profiles with peak heating rate (PHR) as a parameter.

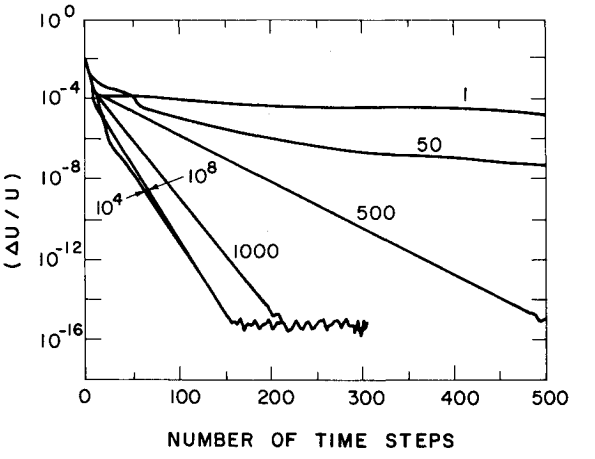

Fig. 5 Time histories of $(\Delta U/U)_{ave}$ for various Courant numbers for MacCormack's scheme, $\mathcal{R}=0.8$, PHR = 0.

parametric studies of both strong nozzle convergence and strong heat addition are considered.

Nozzle Geometry and Heating Profiles

The family of nozzle shapes chosen for the analysis is characterized by a single parameter, the area ratio, $\mathcal{R}$, which is defined as the ratio of the throat area to the inlet area. Some representative nozzle shapes from this family are given in Fig. 2. The converging-diverging portion of the nozzle is defined by a cubic equation preceded by a short, straight section,

$$A_F = 1 \qquad \text{for } X \le 0$$

$$= -2(\mathcal{R}-1)X^3 + 3(\mathcal{R}-1)X^2 + 1 \qquad \text{for } X \ge 0 \qquad (35)$$

where A_F is the local flow area nondimensionalized by the area at the entrance. The distance, X, is nondimensionalized by length of the convergent section of the nozzle.

The heating rate is also defined parametrically to facilitate an ordered investigation. The amount of heat added is designated by the peak heating rate, PHR, which describes the relative level of the heat flux at the peak. Representative heating rate curves for several values of PHR are shown in Fig. 3. The heating rate profile is defined in three segments:

$$Q = -2\text{PHR}\left(\frac{X-X_1}{X_2-X_1}\right)^3 + 3\text{PHR}\left(\frac{X-X_1}{X_2-X_1}\right)^2 \qquad X_1 \le X \le X_2$$

$$= \text{PHR} \qquad X_2 \le X \le X_3$$

$$= 2\text{PHR}\left(\frac{X-X_3}{X_4-X_3}\right)^3 - 3\text{PHR}\left(\frac{X-X_3}{X_4-X_3}\right)^2 + \text{PHR} \qquad X_3 \le X \le X_4 \qquad (36)$$

and is zero elsewhere. For the present calculations, $X_1 = 0.05$, $X_2 = 0.35$, $X_3 = 0.45$, and $X_4 = 0.75$. In these equations, the heating rate is nondimensionalized by the peak heating rate at PHR = 1. The heating rate corresponding to maximum energy input in the laser propulsion application is approximately PHR = 20.

Representative Flowfield Solutions

To quantify the flowfields of interest, the results of two converged solutions are shown in Fig. 4. These calculations are for the same nozzle shape, $\mathcal{R} = 0.8$, but for different rates of heat addition, PHR = 3 and 7. Although the flowfields are qualitatively similar, they represent calculations with very different degrees of difficulty. The results in Fig. 4 for the lower heating rate (PHR = 3) represent a relatively easy calculation in which the solution converges reliably regardless of the algorithm or time step. The results for the higher heating rate represent a more difficult calculation.

The Mach number profiles for these two flowfields are nearly identical, except near the entrance where the Mach number is reduced from approximately 0.06 for the PHR = 3 case to about 0.04 for the PHR = 7 case. This Mach number change occurs because of the reduction in mass flow caused by the increased heat addition. In addition to these Mach number changes, the temperature profile becomes steeper as the heating become stronger. Both of these items make convergence more difficult. Quantitative details on how convergence is affected are given in the next subsection.

Solution Convergence Without Heat Addition

Solution convergence was monitored by keeping track of the change in the flux vector $\Delta U/U$ averaged over the entire flowfield as a function of the number of time steps. All calculations were done with 65 equally spaced points. The convergence results are portrayed by showing the largest component of $\Delta U/U$. For cases without heat addition, this corresponded to the momentum equation. For cases with substantial heat addition, the component from the energy equation was largest. Convergence was defined as $\Delta U/U \le 10^{-12}$. This rigorous convergence criterion ensured mass conservation to four decimal places.

The convergence pattern for MacCormack's implicit scheme for a nozzle with an area ratio $\mathcal{R} = 0.8$ and PHR = 0 (no heat addition) is given in Fig. 5. With only a small change in the nozzle area from the inlet to the throat, the solution convergence extends from a Courant number of unity to 10^8, as suggested by the stability results. (Here, the Courant number is based upon the $u+c$ characteristics and conditions at the throat.) Above 10^4, the convergence rate is essentially independent of Courant number and as the Courant number is reduced below 10^4, the convergence rate decreases.

A map showing the regimes in which MacCormack's scheme converges for this case (as well as several other area

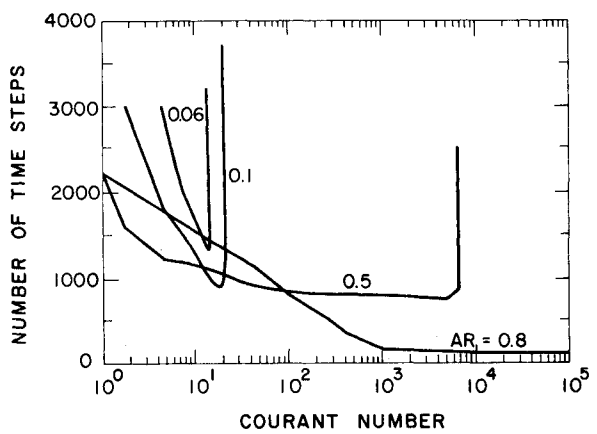

Fig. 6 Convergence of MacCormack's scheme for various area ratios, PHR = 0.

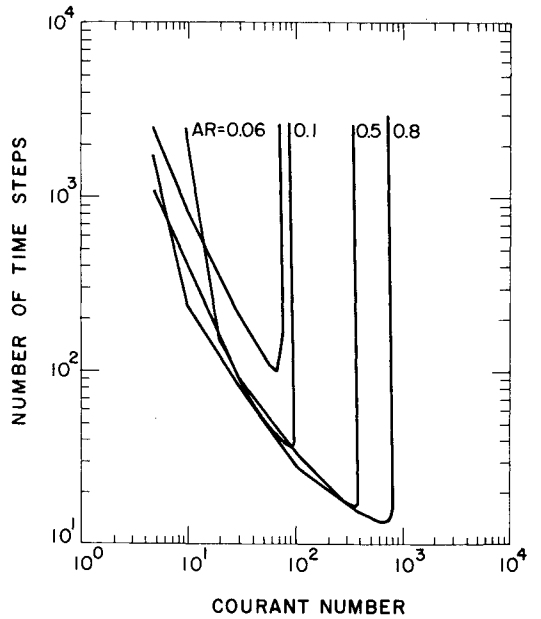

Fig. 7 Convergence of Beam and Warming's Euler implicit scheme for various area ratios, const Δt PHR = 0.

ratios) is shown in Fig. 6. As the nozzle throat area is reduced, there appears an upper maximum on the allowable Courant number above which convergence is very slow and divergence can be expected. The band of Courant numbers for which the best convergence occurs also continues to decrease as the throat area is reduced. In these calculations, a linear Mach number profile passing through unity at the throat and constant stagnation conditions were used as the initial condition for the $\mathcal{R}=0.8$ case. The smaller area ratio cases were all started from a converged solution corresponding to one of the larger area ratio cases. Identical initial conditions were used for MacCormack's and Beam and Warming's methods.

Companion results obtained with Beam and Warming's algorithm for these zero heat cases are shown in Fig. 7. The detailed behavior of the convergence characteristics of this scheme is somewhat different than that observed for MacCormack's scheme. Part of this difference arises because of the stability limitation that occurs at large values of CFL. Each area ratio shows a cutoff CFL beyond which reliable convergence cannot be obtained. (It is, however, noted that rapid convergence was observed in several randomly spaced, narrow bands of CFL above the indicated limits with regions of divergence in between.) These experimentally observed stability limits are compared with the theoretical predictions from Eqs. (26) in Fig. 8. For completeness, several values of explicit artificial viscosity (ϵ_e) are also shown here. The calculations were made with $\epsilon_e=0.6$.

In an effort to obtain better convergence with Beam and Warming's scheme, the largest and smallest area ratio cases were recomputed using a uniform CFL condition (i.e., a different value of Δt) at each grid point. These constant CFL results are shown in Fig 9. As can be seen, there is no major effect of switching from uniform Δt throughout the field to uniform CFL. The uniform CFL procedure is, however, slightly more reliable (converges over a wider range of CFL's) and is slightly more economical.

Solution Convergence with Heat Addition

All of the results for cases with heat addition presented herein have been computed for a nozzle with $\mathcal{R}=0.8$. The initial conditions for cases with heating were again taken as converged solutions from cases with lower heating rates. The effect of the Courant number on the number of steps required for convergence with Beam and Warming's scheme is shown in Fig. 10 for various peak heating rates. With increasing heat addition, the range of Courant numbers for which the method converges continues to diminish. Convergence could be attained up to a PHR slightly above seven, but at higher PHR's, it was no longer possible to obtain converged solutions. MacCormack's algorithm exhibited similar trends, but again its range of convergence was smaller than with Beam and Warming's algorithm. This deterioration is analogous to that observed when decreasing the nozzle area ratio. Decreasing the nozzle area ratio decreases the inlet Mach number and increases the magnitude of the source term in the momentum equation. Correspondingly, increasing the heat addition decreases the inlet Mach number and increases the source term in the energy equation, although this latter source is not coupled to the solution.

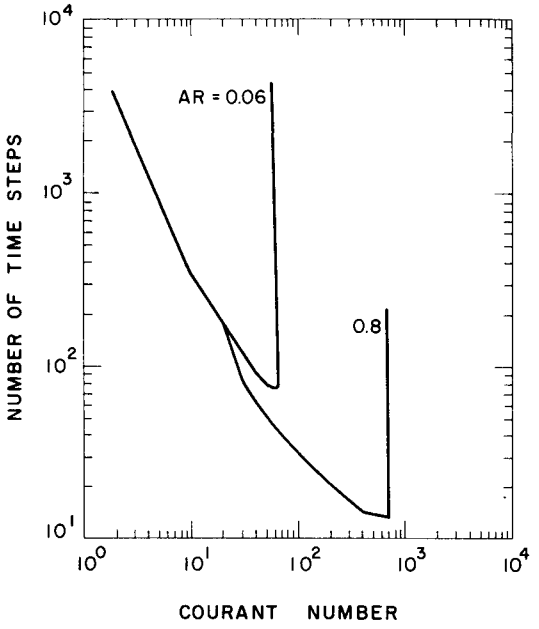

Fig. 9 Convergence of Beam and Warming's Euler implicit scheme for various area ratios, const CFL, PHR = 0.

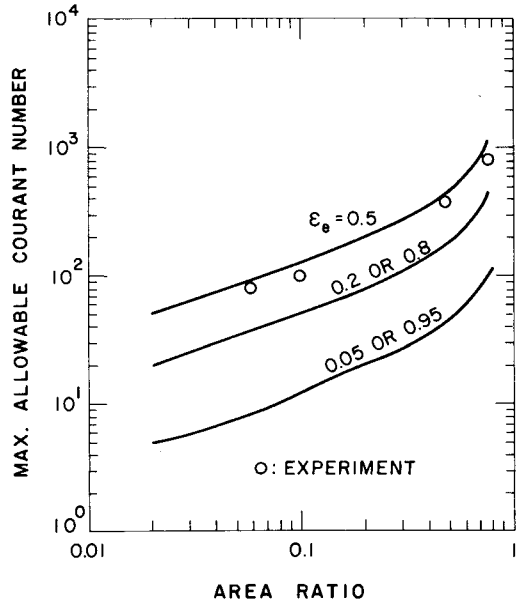

Fig. 8 Maximum allowable Courant number for various area ratios as a function of explicit artificial dissipation. Beam and Warming's Euler implicit scheme.

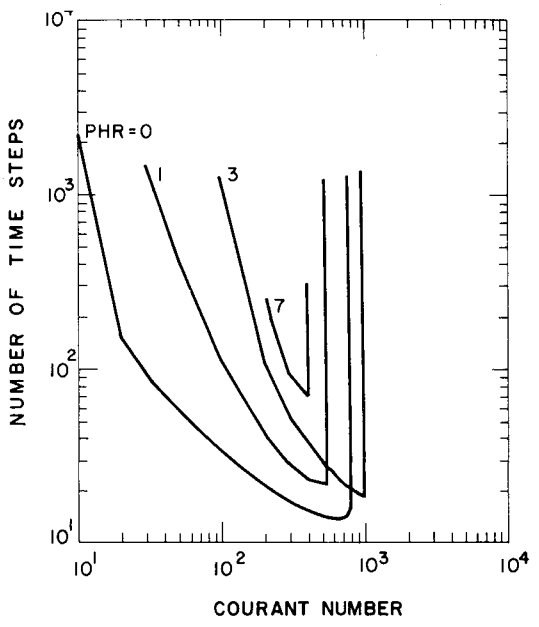

Fig. 10 Convergence of Beam and Warming's Euler implicit scheme for various peak heating rates, $\mathcal{R}=0.8$, const Δt.

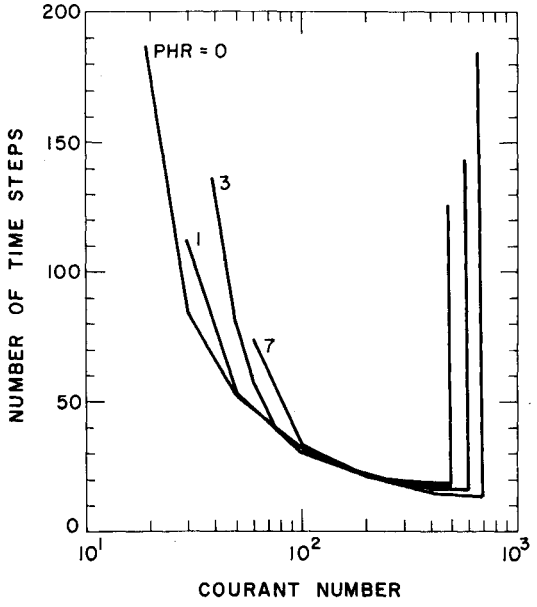

Fig. 11 Convergence of Beam and Warming's Euler implicit scheme for various peak heating rates, $\mathcal{R}=0.8$, const CFL.

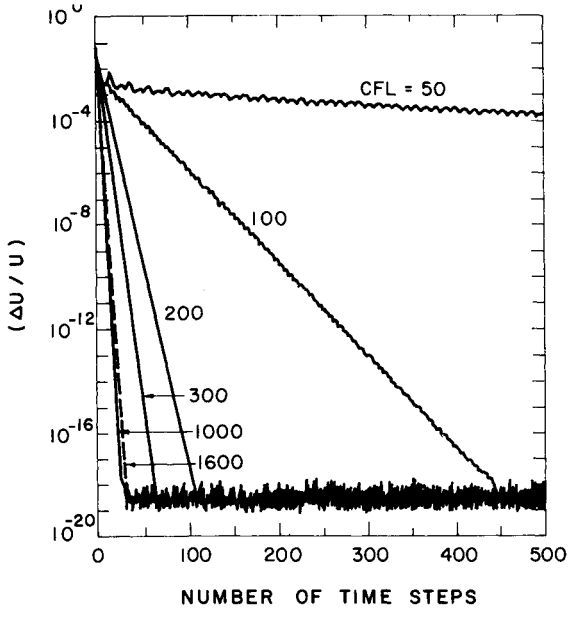

Fig. 12 Time histories of $(\Delta U/U)$ as a function of Courant number for the Euler implicit scheme of Beam and Warming, PHR = 2, $\mathcal{R}=0.8$, const Δt.

The Beam and Warming algorithm with uniform values of CFL was also tried for the heat addition calculations. The results are shown in Fig. 11. Here, we see that, in agreement with stability theory, the convergence of the uniform CFL calculations is almost entirely independent of heat addition. The effectiveness of the variable time step arises because it negates the effect of strongly varying coefficients which are introduced by heat addition. The constant CFL case is more nearly analgous to the locally constant coefficient assumption used in the stability analysis. This removal of the sensitivity of convergence to the presence of heat addition is analogous to the removal of the sensitivity to the effects of strongly varying Jacobians which occur as a result of highly stretched grid mappings.

The time histories of the change in the dependent variable, $\Delta U/U$, with Beam and Warming's algorithm are shown in Fig. 12 for several Courant numbers. These calculations correspond to $\mathcal{R}=0.8$, $PHR=2$, and $\epsilon_e=0.6$. All calculations shown here are convergent, with fastest convergence being obtained at the higher Courant numbers. Calculations at Courant numbers larger than those shown led to rapid divergence. The convergence history exhibited in this figure is typical of the observed at other peak heating rates.

Summary

The effect of the addition of substantial amounts of heat to the flow in a converging-diverging nozzle on the convergence characteristics of implicit schemes has been investigated. When heat is added to the flow, the entrance Mach number is reduced, a significant source term is added to the energy solution, and a steep temperature gradient is produced. All of these effects are detrimental to a numerical scheme but can be overcome if proper care is exercised.

Results show that when proper artificial viscosity is used along with Euler implicit differencing in time, Beam and Warming's scheme converges for a wider range of parameters than does MacCormack's. However, this comparison is not completely consistent in that different upstream boundary conditions were used for the two methods. For Beam and Warming's case, method of characteristic boundary conditions was used, while for the MacCormack case, extrapolation was used. The reason for this difference was the difficulty of applying method of characteristics boundary conditions to MacCormack's scheme without destroying its bidiagonal character. Although more optimum boundary conditions might have been found for MacCormack's scheme, representative tests of an analogous extrapolation procedure in Beam and Warming's algorithm did not alter this conclusion.

Even though Beam and Warming's algorithm converges somewhat more reliably than the MacCormack algorithm it still shows substantial deterioration in convergence as more and more heat is added unless nonuniform time steps are used. The use of uniform CFL values at every grid point (instead of uniform Δt), however, makes the convergence nearly independent of the amount of heat addition. This is in agreement with stability theory that says the heat source does not effect convergence. It is important to note that although nonuniform time steps were tested only for Beam and Warming's algorithm, there is no reason to expect that they would not also behave in the same manner with MacCormack's scheme.

A major difference between the two schemes is that Beam and Warming's algorithm requires the addition of artificial viscosity to maintain stability in a converging nozzle, whereas MacCormack's scheme does not. The viscosity added to Beam and Warming's method decreases to zero as the fourth power of the grid spacing and shows a weak dependence on the time step. The observed convergence patterns with Beam and Warming's scheme are in excellent agreement with the stability predictions.

Finally, it is noted that the use of real gas properties has little effect on convergence and reliability. Detailed calculations (not shown) demonstrated that although computation times are increased somewhat because of the additional calculations, the number of iterations required for convergence is unaffected.

Acknowledgment

Portions of this work were sponsored by the Air Force Office of Scientific Research under Contract AFOSR 82-0196.

References

[1]Jones, L. W. and Keefer, D. R., "NASA's Laser Propulsion Project," *Astronautics & Aeronautics*, Vol. 20, Sept. 1982, p. 66.

[2]Raizer, Yu. P., "Subsonic Propagation of a Light Spark and Threshold Conditions for the Maintenance of Plasma by Radiation," *Soviet Physics JETP*, Vol. 31, No. 6, 1970, p. 1148.

[3]Batteh, J. H. and Keefer, D. R., "Two-Dimensional Generalization of Raizer's Analysis for the Subsonic Propagation of Laser Sparks," *IEEE Transactions on Plasma Science*, Vol. PS-2, Sept. 1974.

[4]Kemp, N. H. and Root, R. G., "Analytical Study of Laser-Supported Combustion Wave in Hydrogen," *Journal of Energy*, Vol. 3, Jan.-Feb. 1979, pp. 40-49.

[5]Gulati, A. and Merkle, C. L., "The Absorption of Electromagnetic Radiation in an Advanced Propulsion System," *Journal of Spacecraft and Rockets*, Vol. 21, Jan.-Feb. 1984, pp. 101-107.

[6]Beam, R. M. and Warming, R. F., "An Implicit Factored Scheme for the Compressible Navier-Stokes Equations," *AIAA Journal*, Vol. 16, April 1978, pp. 393-402.

[7]MacCormack, R. W., "A Numerical Method for Solving the Equations of Compressible Viscous Flow," *AIAA Journal*, Vol. 20, Sept. 1982, p. 1275.

[8]Lomax, H., "Some Prospects for the Future of Computational Fluid Dynamics," *AIAA Journal*, Vol. 20, Aug. 1982, pp. 1033-1043.

[9]Steger, J. L. and Warming, R. F., "Flux Vector Splitting of the Inviscid Gas Dynamic Equations with Application to Finite-Difference Methods," *Journal of Computational Physics*, Vol. 40, April 1981, pp. 263-293.

[10]Briley, W. R. and McDonald, H., "Solution of Multi-Dimensional Compressible Navier-Stokes Equations by a Generalized Implicit Method," *Journal of Computational Physics*, Vol. 24, Aug. 1977, pp. 372-397.

[11]Warming, R. F. and Beam, R. M., "On the Construction and Application of Implicit Factored Schemes for Conservation Laws," *SIAM-AMS Proceedings of the Symposium on Computational Fluid Mechanics*, Vol. 11, 1978, pp. 85-129.

[12]Steger, J. L. and Bailey, H. E., "Calculation of Transonic Aileron Buzz," *AIAA Journal*, Vol. 18, March 1980, pp. 249-255.

[13]Richtmeyer, R. D. and Morton, K. W., *Difference Methods for Initial-Value Problems*, 2nd ed., John Wiley & Sons, New York, 1969.

[14]MacCormack, R. W., "The Effect of Viscosity in Hypervelocity Impact Cratering," AIAA Paper 69-354, April-May 1969.

[15]White, M. E. and Anderson, J. D. Jr., "Application of MacCormack's Implicit Method to Quasi-One-Dimensional Nozzle Flows," AIAA Paper 82-0992, June 1982.

[16]Rai, M. M. and Chausee, D. S., "New Implicit Schemes and Implicit Boundary Conditions," AIAA Paper 82-0123, Jan. 1983.

[17]Chakravarthy, S. R., "Euler Equations—Implicit Schemes and Implicit Boundary Conditions," AIAA Paper 82-0228, Jan. 1982.